RSC Advances

ROYAL SOCIETY OF CHEMISTRY

www.rsc.org/advances

Adjusting Electronic Properties of Silicon Carbide Nanoribbons by Introducing Edge Functionalization

Yanqiong He[1], Peng Zhang[1,3,4,*], Xiuli Hou[1], Jiajia Xu[1], Meiqi Wang[1], Yansen Wu[1], Jiacheng Qu[1] and Mingdong Dong[2,*]

[1]*Institute for Advanced Materials, and School of Materials Science and Engineering, Jiangsu University, Zhenjiang 212013, China,*

[2]*Center for DNA Nanotechnology (CDNA), interdisciplinary Nanoscience Center (iNANO), Aarhus University, DK-8000 Aarhus, Denmark,*

[3]*Key Laboratory of Automobile Materials, Ministry of Education, and Department of Materials Science and Engineering, Jilin University, Changchun 130022, China,*

[4]*State Key Laboratory of Metastable Materials Science and Technology, Yanshan University, Qinhuangdao 066004, China.*

Abstract: The structural and electronic properties of silicon carbide nanoribbons (SiC NRs) with edges passivated by hydrogen and halogens are calculated based on the density functional theory. It is found that the band gap (E_g) values of armchair SiC NRs decrease as the atomic number of hydrogen and halogen elements increases. However the effect of edge functionalization on the E_g of zigzag SiC NRs is very small. This is because the energy levels of conduction band minimum of armchair SiC NRs shift to lower energy region by introducing hydrogen and halogen atoms, while the energies of valence band maximum are barely affected. Our results provide a theoretical guideline to adjust the electronic properties of SiC NRs.

* Corresponding author. Email: zhangpjlxb@ujs.edu.cn, dong@inano.au.dk

1. Introduction

Nanoribbons (NRs), in particular, graphene NRs (GNRs), boron nitride NRs, and silicon carbide NRs (SiC NRs), have attracted lots of attention in recent years, due to their exciting properties and potential applications in several fields like optics, electronics, opto-electronics, spintronics, and so on.[1-4] These applications of NRs mainly depend on their electronic structures and edge configurations.[5,6] As one of the most investigated NRs, GNRs can be either metallic or semiconducting depending on the structure of the edges.[7,8] As proved by the previous studies on GNRs, the electronic properties can be finely tuned by different methods, namely, passivation,[9,10] defect,[11] substitution,[12] external electric fields,[13] heterojunctions,[14,15] and so on. The hydrogen passivated GNRs have nonzero band gaps.[16] However, transverse electric field or chemical decoration can turn zigzag GNRs to half-metals,[10,13] which make them good candidates for spintronic applications.

SiC, a binary compound of carbon and silicon, has attracted extensive research interest due to its unique properties. Two-dimensional (2D) SiC with a honeycomb structure has been predicted to be energetically stable based on density functional theory (DFT) calculations.[17,18] The 2D SiC nanosheets with single atom thickness have been successfully synthesized through the sonication of alpha-phase SiC powders in N-methylpyrrolidone or isopropyl alcohol.[19] It would be noted that, although the 2D SiC nanosheet is a semiconductor, the corresponding one-dimensional zigzag SiC (ZSiC) NRs with bare edges exhibit intrinsic half-metallic behaviors.[20] The electronic properties of SiC NRs depend on their width

and edge configurations.[21,22] The armchair SiC (ASiC) NRs passivated by hydrogen (ASiC-H) are nonmagnetic semiconductors, while the ZSiC NRs with width narrower than 4 nm passivated by hydrogen (ZSiC-H) present half-metallic behavior.[23] The ZSiC NRs can transform into a metal/semiconductor when the edges are terminated by O/S atoms.[20] Under an external electric field, the ZSiC-H NRs convert from magnetic semiconductors to ferromagnetic metals and the magnetization direction depends on the field direction.[24] In addition, the magnetization and magnetization direction of ZSiC NRs can be manipulated by carriers (hole and electron).[25]

Although tremendous efforts have been devoted to investigate the effect of the functionalization on the electronic properties of graphene and GNRs,[9,10,25] a complete picture of the effect of edge functionalization on the electronic properties of SiC NRs has not been obtained, which is very important for designing and fabricating electronic nanodevices. In this paper, ASiC and ZSiC NRs with edges passivated by H and halogen atoms are studied based on DFT. It is found that the effect of edge functionalization on band gaps (E_g) of ZSiC NRs is very small, while E_g of ASiC NRs can be effectively modified and decrease as the atomic numbers of corresponding hydrogen and halogen atoms increase. This is because the energy of conduction band minimum (CBM) shifts to lower energy region due to the introduction of hydrogen and halogen atoms, while the energy of valence band maximum (VBM) is barely affected.

2. Computational Methods

All calculations are performed within DFT framework as implemented in DMol[3]

code.[26,27] The generalized gradient approximation (GGA) with the Perdew-Burke-Enzerhof (PBE) method is used to describe the exchange and correlation interactions.[28] All electron relativistic core treatment and double numeric plus polarization (DNP) basis set are adopted for the spin-unrestricted computations.[29] The structures are optimized and the electronic properties are calculated using the Monkhorst-Pack 1×1×1 k-point mesh for Brillouin zone sampling. The convergence tests for k-point are summarized in Table 1, which shows that the bond lengths and the E_g are converged when the used k-point is larger than 1×1×1. The real space global cutoff radius is set to be 4.6 Å. The convergence tolerance of energy is 1×10^{-5} Ha (1 Ha = 27.2114 eV), maximum force is 0.002 Ha/Å, and maximum displacement is 0.005 Å. A smearing of 0.005 Ha to the orbital occupation is applied to achieve accurate electronic convergence. It is noteworthy that the standard DFT calculations with GGA-PBE functional might underestimate the E_g value.[30] It has been shown that more accurate physical results and behavior can be obtained by using hybrid functional or DFT + U calculations.[31,32] The hybrid functional involves a portion of the exact Hartree-Fock exchange and reduces some of the shortcomings of the classical DFT functional such as the self-interaction error.[33,34] The DFT + U approach introduces an on-site correction in order to describe strong correlated. Hubbard U has been mostly added on the localized *d* and *f* electrons, which is not appropriate in our case.[35,36] Therefore, we compare our results with that based on hybrid functional. During electronic calculations by the hybrid sX-LDA functional in CASTEP code,[37,38] Norm-conserving pseudopotential with the energy cutoff of 850 eV is used.

The SiC NR width (W) is defined as the number of dimer lines along the ribbon non-periodic direction for an ASiC-X NR and the number of zigzag chains perpendicular to the ribbon non-periodic direction for a ZSiC-X NR, as schematically shown in Figs. 1(a) and (b), respectively. The edge Si and C atoms with active dangling σ bonds are passivated by hydrogen or halogen atoms (F, Cl and Br). These structures are referred to as ASiC-X or ZSiC-X NRs, where the postfix X represent the corresponding H, F, Cl and Br atoms, respectively. The minimal distances between the SiC NRs and their mirror images are set as 15 Å, which is sufficiently large to avoid the interaction between them.

3. Results and Discussion

The structural stability of edge functionalized SiC NRs is evaluated firstly. The average formation energy E_f is determined by $E_f = (E_{A/ZSiC} + nE_{X2}/2 - E_{A/ZSiC-X})/n$, where E_{X2}, $E_{A/ZSiC}$, $E_{A/ZSiC-X}$ and n are the total energies of corresponding hydrogen/halogen molecules, SiC NRs with bare edges, SiC NRs with edges passivated and the number of hydrogen/halogen atoms, respectively. By these definitions, the positive E_f values correspond to exothermic adsorption processes, indicating the stable structures. As shown in Table 1, all E_f values are positive, suggesting H, F, Cl and Br atoms can adsorb on SiC NRs stably. This is consistent with the case of silicene.[39] The Si-X and C-X bond lengths are independent from the ribbon W and increase with the atomic numbers of hydrogen and halogen atoms. The structural properties and E_g of ASiC-H and ZSiC-H SiC NRs have shown consistency with previous theoretical studies,[23] demonstrating the correctness of our approach.

The variations of E_g with W for A(Z)SiC-X NRs are shown in Fig. 2. For NRs wider than 0.9 nm (W = 7 for ASiC-X and W = 4 for ZSiC-X), the change of the E_g is very small. This is because the proportion of edge atoms becomes smaller as the W increases, suggesting the size effect becomes weaker.[40,41] Importantly, E_g values of ASiC-X NRs decrease as the atomic numbers of X atoms increase, while those of ZSiC-X NRs are nearly unchanged. This is different from that of GNRs, where the E_g value is almost the same when edge is passivated by F, Cl and Br.[9]

The band structures, spatial distribution of VBM and CBM of ASiC-X are shown in Fig. 3. The ASiC-X NRs with W = 7 are taken as an example to discuss here. Note that the energy wave function at Γ and K points is a little different and the energy band is relatively flat, suggesting the localized property of electron states in ASiC-X NRs. The bandwidth or dispersion of a band (the energy difference between the highest and lowest levels in a band) is determined by the overlap between the interacting orbitals. The greater the overlap between neighbors, the greater the band width is. The energy of VBM remains unchanged as the increase of the atomic numbers of hydrogen and halogen atoms, while the CBM shifts to lower energy region, resulting in the decrease of E_g values. The E_g of silicon nanowires is also adjusted by H and halogens passivated, but the CBM and VBM are both changed distinctly.[42] As the minimum energy value of conduction band at the K point reduces more rapidly than that at the Γ point from ASiC-H to ASiC-Br, the CBM is transferred from Γ point to K point and the direct E_g of ASiC-H and ASiC-F is changed to the indirect E_g of ASiC-Cl and ASiC-Br. From Fig.3, it can be found that passivated

atoms influence the distribution of CBM and VBM, and more electron states from Cl and Br contribute to the conduction band. The CBM and VBM of ASiC-H are determined by Si and C atoms, respectively. By contrast, halogen atoms affect the orbitals distribution of the Si and C atoms, which are responsible for the changes of CBM, VBM, and E_g of the ASiC-X NRs. As shown in Table 1, the structural and electrical properties of ASiC-X NRs with W = 10 are also investigated, which are in good agreement with that with W = 7.

Considered that the GGA-PBE method might underestimate the band gap values,[30] the hybrid sX-LDA functional with CA-PZ has also been performed in this work. As shown in Table 1, although the E_g values of ASiC-X NRs based on sX-LDA are slightly larger than that based on GGA-PBE, the effect of edge functionalization is the same. The E_g value of ASiC-X NRs increases as the atomic number of X decreases.

In order to gain more insight into the nature of the electronic structures of ASiC-X NRs, the partial density of states (PDOS) of the edge Si/C atoms and X atoms are shown in Fig. 4. Only the PDOS of the edge Si/C atoms are displayed, because the edge Si/C atoms contribute the most electrons in the energy region around the Fermi level, as shown in the spatial distribution of VBM and CBM in Fig. 3. Near the Fermi level, few electrons from the *s* orbital are available and *p* electrons play the predominant role. Thus, only *p* orbitals are considered here. As shown in Fig. 4, the CBM of ASiC-H is determined by the Si-3*p* orbital and VBM is determined by C-2*p* electrons, while the electrons of H atoms do not involve. With the increasing of the

atomic numbers of halogen atoms, the C-2*p* electrons are almost constant, indicating the unchanged VBM. On the contrary, Si-3*p* orbital in the conduction band shifts downward and gets close to the Fermi level, suggesting the decline of the CBM. In addition, more electrons of halogen atoms contribute to the VBM. The F states mainly locate in the lower energy region of the valence band in ASiC-F, while Cl and Br states shift to higher energy region in ASiC-Cl and ASiC-Br. At the same time, the effect of halogen atoms on the CBM and conduction band becomes larger and larger as the increase of atomic number. Both effects of Si and halogen atoms result in the variation of CBM and the decrease of E_g. These are in good agreement with the variation of band structures shown in Fig. 3, i.e. the CBM of ASiC-X NRs shift to lower energy region by the introduction of hydrogen and halogen atoms, while the VBM are barely affected.

The Hirshfeld population charge distribution of ASiC-X NRs is shown in Table 2, which provides a different point to understand the interactions between ASiC NRs and X atoms. The charge of the edge Si or C atoms decreases as the electronegativity of the corresponding X atom decreases, and close to the interior Si and C atoms. The variations of charges for Si and C atoms in second dimer lines near edges are very small, suggesting that X atoms have little effect on the interior atoms and the energy band around the Fermi level of ASiC-X NRs are mainly contributed by the edge atoms. This is consistent with the spatial distributions of CBM and VBM in Fig. 3. Note that the charge variation of X-Si and C-Si-ed atoms from ASiC-F to ASiC-Br is not monotonously. This is due to the different adsorption structure of halogen on

ASiC-X, as shown in Fig.3. As the atomic diameter increases from F to Br, the deformation of the edge becomes obviously. The relaxation of the edge results in the non-systematically change of charge distributions on X-Si and C-Si-ed. Due to the relative large electronegativity difference between Si and halogen, the Si/C-X (F, Cl, Br) bonds exist ionic characterization to some extent and the ionic characterization becomes weaker as the electronegativity decreases from F to Br. The electronegativity of H is between the Si and C, and their electronegativity values are close to each other. Si(C)-H bonds intend more covalent character instead of ionic property. (The Pauling electronegativity value of the F, Cl, Br, H, Si, C are 3.98, 3.16, 2.96, 2.2, 1.98, 2.55, respectively).[43] The partly ionic characteristic of the Si/C-X (F, Cl, Br) bonds diminishes the electron population in the bonding orbital of Si, weakens Si-C bonding, and decreases the bonding-antibonding splitting, leading to the variation of electron distribution and E_g.

It is observed that the effect of edge functionalization on the E_g of ZSiC-X NRs is different from that of ASiC-X NRs. The variation of E_g is very small when edge is passivated. When W is larger than 3, the E_g values are almost the same and close to zero regardless of the passivated atoms. As shown in Fig. 5, the band structures of four ZSiC-X NRs are similar to each other. VBM and CBM of ZSiC-X NRs come from the C and Si atoms. Different from the ASiC NRs, which have two edges with Si and C atoms arranged alternately, one side of ZSiC NRs is Si atom edge and the other is C atom edge. Since the E_g values are always determined by the electron states of edge atoms, the different edge configuration results in the different effect of edge

functionalization on the electronic properties of SiC NRs. The edge configuration of ASiC NRs is similar with the semiconductor SiC nanosheet, which shows an opened gap.[23] However, the edge configuration of ZSiC NRs is analogous to zero gap semimetal silicene[39] and graphene,[44] showing a tiny E_g.

4. Conclusions

In summary, the electronic properties of armchair/zigzag SiC NRs with edges functionalized are investigated based on the DFT. The change of E_g is very small when the ribbon width is larger than 0.9 nm. The E_g value of ASiC-X NRs decreases in the order of H, F, Cl and Br, while that of ZSiC-X NRs is nearly unchanged. For ASiC NRs, the CBM originates from the Si atoms and hydrogen/halogen atoms, and shifts to lower energy region due to the introduction of adsorbed atoms, while VBM contributed mostly by the C atoms keep nearly constant, resulting in the decrease of E_g. The VBM of ASiC-X NRs are all at the Γ point, while the CBM changes from Γ point for ASiC-H and ASiC-F to K point for ASiC-Cl and ASiC-Br, leading to the direct-indirect E_g transition.

Acknowledgements

This work was financially supported by Natural Science Foundation of Jiangsu (No. SBK201341900), China Postdoctoral Science Foundation (No. 2013M541611 and 2014M550270), the Senior Intellectuals Fund of Jiangsu University (No. 12JDG094 and 13JDG032), Danish National Research Foundation, the Danish Ministry of Science, Technology, and Innovation through Center for DNA Nanotechnology

(CDNA), interdisciplinary Nanoscience Center (iNANO). The authors also like to thank Professor Qing Jiang (Jilin University) for computer resources and helpful discussions.

Table 1. Structural and electronic properties of ASiC-X and ZSiC-X NRs. l_{Si-X}, l_{C-X} (Å), E_f, E_{CBM}, E_{VBM} and E_g (eV) stand for the Si-X and C-X bond lengths, formation energy per hydrogen/halogen atom, energy of CBM and VBM and E_g.

	A/ZSiC-X	l_{Si-X}	l_{C-X}	E_f	E_{CBM}	E_{VBM}	E_g	$(E_g)^c$
W=7	ASiC-H	1.489	1.094	2.037	–2.644	–5.010	2.365	2.930
	(ASiC-H)[a]	1.489	1.094	2.044	–2.645	–5.014	2.369	
	(ASiC-H)[b]	1.489	1.094	2.044	–2.645	–5.014	2.369	
	ASiC-F	1.596	1.380	4.298	–3.117	–5.285	2.169	2.804
	ASiC-Cl	2.133	1.733	2.197	–3.350	–5.198	1.849	2.602
	ASiC-Br	2.462	1.921	1.737	–4.102	–5.319	1.217	2.094
	ZSiC-H	1.488	1.095	1.974	–3.936	–4.038	0.103	
	ZSiC-F	1.606	1.378	4.343	–3.975	–4.114	0.138	
	ZSiC-Cl	2.037	1.751	2.571	–3.940	–4.056	0.115	
	ZSiC-Br	2.203	1.928	2.035	–3.840	–3.863	0.023	
W=10	ASiC-H	1.489	1.094	1.921	–2.675	–5.032	2.357	
	ASiC-F	1.597	1.380	4.182	–3.057	–5.257	2.200	
	ASiC-Cl	2.132	1.734	2.094	–3.153	–5.178	2.025	
	ASiC-Br	2.462	1.921	1.632	–3.701	–5.289	1.589	

[a]k-ponint is 2×2×2. [b]k-ponint is 4×4×4. [c]based on sX-LDA in CASTEP code.

Table 2. Hirshfeld charge distribution of ASiC-X NRs with W = 7. The corresponding atoms index is shown in Fig. 1.

	Si-ed	C-ed	Si-C-ed	C-Si-ed	X-Si	X-C
ASiC-F	0.4250	–0.1775	0.3132	–0.3285	–0.1477	–0.0958
ASiC-Cl	0.3399	–0.2589	0.3078	–0.3165	–0.1050	0.0198
ASiC-Br	0.3028	–0.2760	0.3042	–0.3210	–0.1381	0.1170
ASiC-H	0.3272	–0.3055	0.3285	–0.3288	–0.0516	0.0292

Captions:

Fig. 1. The geometric structures of armchair SiC (ASiC) NR (a) and zigzag SiC (ZSiC) NR (b) passivated by H atoms with W = 7.

Fig. 2. The variation of band gap (E_g) for ASiC-X (a) and ZSiC-X (b) NRs as a function of the ribbon width W.

Fig. 3. Band structures and spatial distributions of the conduction band minimum (CBM) and the valence band maximum (VBM) at the Γ point for (a) ASiC-H, (b) ASiC-F, (c) ASiC-Cl and (d) ASiC-Br with W = 7. (e) The variation of band gap (E_g), CBM, VBM and Fermi level for ASiC-X NRs with W = 7. The Fermi level is labeled with a red dashed line. The isosurface value is 0.030 e/ $Å^3$.

Fig. 4. Partial density of states (PDOS) for functionalized ASiC-X NRs with W = 7. Si-ed/C-ed represent the edge Si/C atoms. X-Si/X-C represent the corresponding H, F, Cl, Br adsorbed on SiC NRs. The Fermi level is labeled with a red dashed line.

Fig. 5. Band structures and spatial distributions of the conduction band minimum (CBM) and the valence band maximum (VBM) at the Γ point for (a) ZSiC-H, (b) ZSiC-F, (c) ZSiC-Cl and (d) ZSiC-Br with W = 7.

Fig. 1

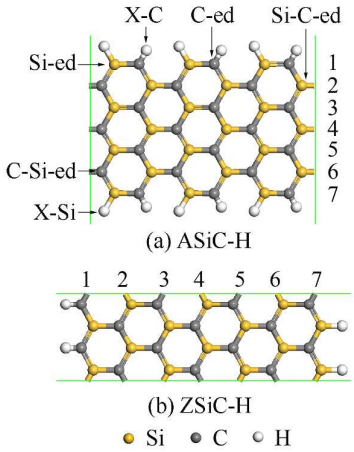

Fig. 2

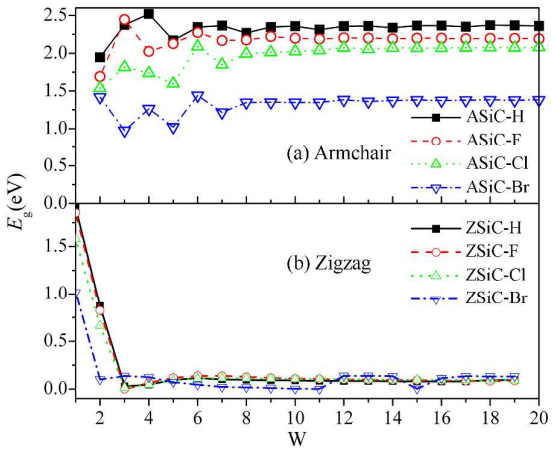

Fig. 3

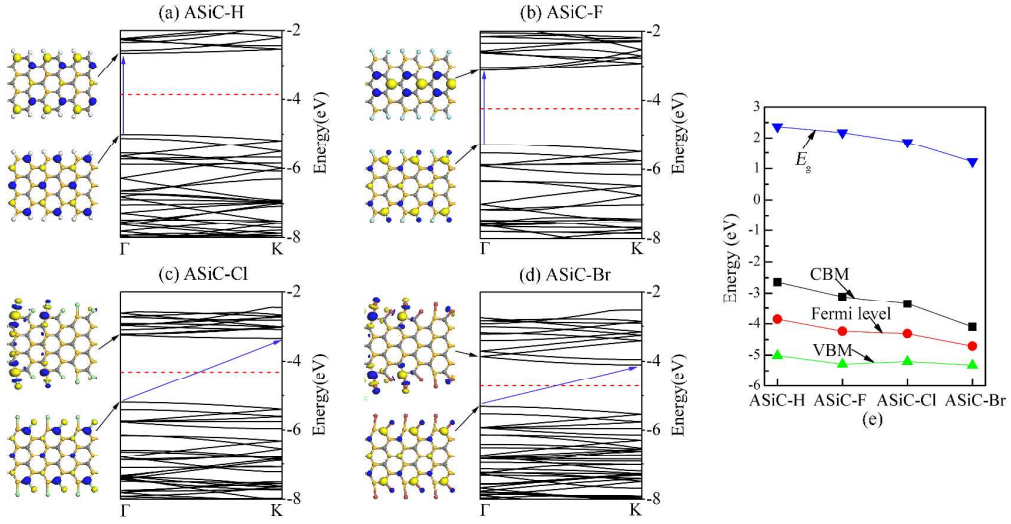

Fig. 4

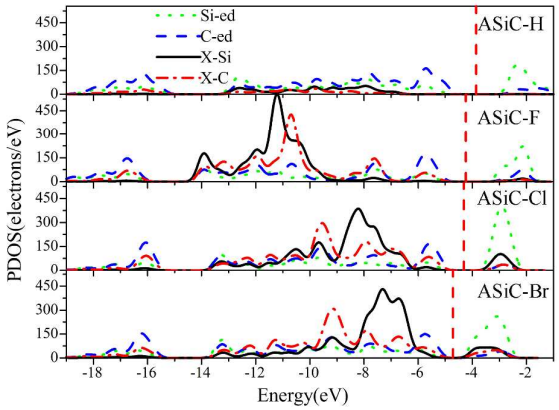

Fig. 5

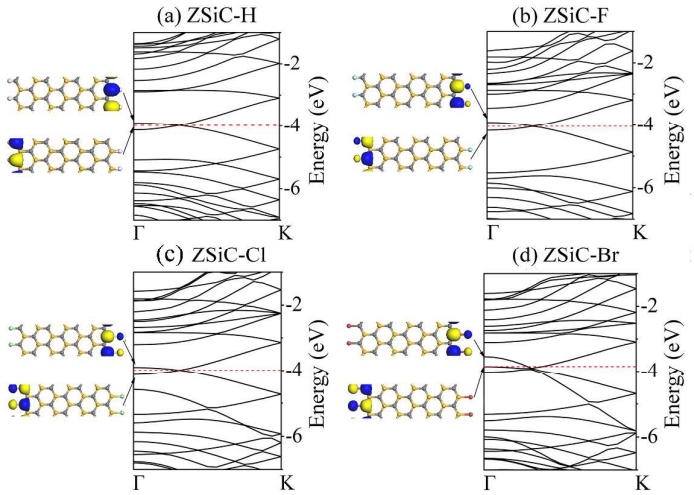

References

1 Y. W. Son, M. L. Cohen and S. G. Louie, *Nature*, 2006, **444**, 347-349.

2 M. Han, B. Özyilmaz, Y. Zhang and P. Kim, *Phys. Rev. Lett.*, 2007, **98**, 206805.

3 H. Zeng, C. Zhi, Z. Zhang, X. Wei, X. Wang, W. Guo, Y. Bando and D. Golberg, *Nano Lett.*, 2010, **10**, 5049-5055.

4 S. Dutta and S. K. Pati, *J. Mater. Chem.*, 2010, **20**, 8207-8223.

5 Y. F. Zhu, Q. Q. Dai, M. Zhao and Q. Jiang, *Sci. Rep.*, 2013, **3**, 1524.

6 M. Terrones, A. R. Botello-Méndez, J. Campos-Delgado, F. López-Urías, Y. I. Vega-Cantú, F. J. Rodríguez-Macías, A. L. Elías, E. Muñoz-Sandoval, A. G. Cano-Márquez and J. C. Charlier, *Nano Today*, 2010, **5**, 351-372.

7 K. Nakada, M. Fujita, G. Dresselhaus and M. S. Dresselhaus, *Phys. Rev. B*, 1996, **54**, 17954-17961.

8 V. Barone, O. Hod and G. E. Scuseria, *Nano Lett.*, 2006, **6**, 2748-2754.

9 P. Wagner, C. P. Ewels, J. J. Adjizian, L. Magaud, P. Pochet, S. Roche, A. Lopez-Bezanilla, V. V. Ivanovskaya, A. Yaya, M. Rayson, P. Briddon and B. Humbert, *J. Phys. Chem. C*, 2013, **117**, 26790-26796.

10 Z. Li, J. Yang and J. G. Hou, *J. Am. Chem. Soc.*, 2008, **130**, 4224-4225.

11 Q. Q. Dai, Y. F. Zhu and Q. Jiang, *J. Phys. Chem. C*, 2013, **117**, 4791-4799.

12 S. Dutta and S. K. Pati, *J. Phys. Chem. B*, 2008, **112**, 1333-1335.

13 E. J. Kan, Z. Li, J. Yang and J. G. Hou, *Appl. Phys. Lett.*, 2007, **91**, 243116.

14 Z. Yu, M. L. Hu, C. X. Zhang, C. Y. He, L.Z. Sun and J. Zhong, *J. Phys. Chem. C*, 2011, **115**, 10836-10841.

15 Y. Liu, X. Wu, Y. Zhao, X.C. Zeng and J. Yang, *J. Phys. Chem. C*, 2011, **115**, 9442-9450.

16 Y. W. Son, M. L. Cohen and S. G. Louie, *Phys. Rev. Lett.*, 2006, **97**, 216803.

17 L. Yuan, Z. Li and J. Yang, *Phys. Chem. Chem. Phys.*, 2013, **15**, 497-503.

18 C. Freeman, F. Claeyssens, N. Allan and J. Harding, *Phys. Rev. Lett.*, 2006, **96**, 066102.

19 S. S. Lin, *J. Phys. Chem. C*, 2012, **116**, 3951-3955.

20 A. Lopez-Bezanilla, J. Huang, P.R.C. Kent and B.G. Sumpter, *J. Phys. Chem. C*, 2013, **117**, 15447-15455.

21 P. Lou, *J. Mater. Chem. C*, 2013, **1**, 2996-3003.

22 P. Lou and J. Y. Lee, *J. Phys. Chem. C*, 2009, **113**, 12637-12640.

23 L. Sun, Y. Li, Z. Li, Q. Li, Z. Zhou, Z. Chen, J. Yang and J.G. Hou, *J Chem. Phys.*, 2008, **129**, 174114.

24 P. Lou and J. Y. Lee, *J. Phys. Chem. C*, 2009, **113**, 21213-21217.

25 P. Lou and J. Y. Lee, *J. Phys. Chem. C*, 2010, **114**, 10947-10951.

26 B. Delley, *J. Chem. Phys.*, 1990, **92**, 508-517.

27 B. Delley, *J. Chem. Phys.*, 2000, **113**, 7756-7764.

28 J. P. Perdew, K. Burke and M. Ernzerhof, *Phys. Rev. Lett.*, 1996, 77, 3865-3868.

29 D. D. Koelling and B. N. Harmon, *J. Phys. C: Solid State Phys.*, 1977, **10**, 3107.

30 X. Li, X. Wu, X. C. Zeng, J. L. Yang, *ACS Nano*, 2012, **6**, 4104-4112.

31 P. Lazar, R. Zbořil, M. Pumera and M. Otyepka, *Phys. Chem. Chem. Phys.*, 2014, **16**, 14231-14235.

32 R. Long and N. J. English, *Chem. Phys. Lett.*, 2010, **498**, 338-344.

33 A. J. Cohen, P. Mori-Sanchez and W. T. Yang, *Chem. Rev.*, 2012, **112**, 289-320.

34 F. Karlický, P. Lazar, M. Dubecký and M. Otyepka, *J. Chem. Theory Comput.*, 2013, **9**, 3670-3676.

35 M. Cococcioni and S. de Gironcoli, *Phys. Rew. B*, 2005, **71**, 035105.

36 S. Lany and A. Zunger, *Phys. Rew. B*, 2005, **72**, 035215.

37 Y. F. Zhu, N. Zhao, J. S. Lian and Q. Jiang, *J. Phys. Chem. C*, 2014, **118**, 2385-2390.

38 T. H. Wang, Y. F. Zhu and Q. Jiang, *Carbon*, 2014, DOI: 10.1016/j.carbon.2014.05.048.

39 N. Gao, W. T. Zheng and Q. Jiang, *Phys. Chem. Chem. Phys.*, 2012, **14**, 257-261.

40 Q. Jiang and H. M. Lu, *Surf. Sci. Rep.*, 2008, **63**, 427-464.

41 Q. Jiang, J. C. Li, and B. Q. Chi, *Chem. Phys. Lett.*, 2002, **366**, 551-554.

42 R. Q. Zhang, X.M. Liu, Z. Wen and Q. Jiang, *J. Phys. Chem. C*, 2011, **115**, 3425-3428.

43 http://www.webelements.com/.

44 A. H. C. Neto and K. Novoselov, *Rep. Prog. Phy*., 2011, **74**, 082501.